Lin et al. *Zool. Res.* 2026, 47(1): 279−288
https://doi.org/10.24272/j.issn.2095-8137.2025.313
https://cstr.cn/32248.14.zr.2025.313

ZR | Zoological Research

Article Open Access

Multiple etiological agents associated with the deaths of trafficked pangolins

Xian-Dan Lin[1,2,#], Shuo-Wei Quan[1,#], Jia-Xin Lv[1,#], Ming-Qiu Liu[1], Yuan-Yuan Pei[1], Xiang Liu[1], Xiu-Qi Luo[1], Hai-Feng Meng[3], Yan-Mei Chen[1,*], Yong-Zhen Zhang[1,*]

[1] *State Key Laboratory of Genetics and Development of Complex Phenotypes*, *School of Life Sciences and Human Phenome Institute*, *Greater Bay Area Institute of Precision Medicine (Guangzhou)*, *Fudan University*, *Shanghai* 200438, *China*

[2] *Wenzhou Center for Disease Control and Prevention (Wenzhou Health Supervision Institution)*, *Wenzhou*, *Zhejiang* 325035, *China*

[3] *Jinhua Wildlife Rescue Station*, *Jinhua*, *Zhejiang* 321000, *China*

ABSTRACT

Pangolins represent the most heavily trafficked mammal globally and harbor diverse microorganisms, raising the concern that illegal trade increases their susceptibility to infectious diseases and facilitates the spread of zoonotic pathogens. In this study, internal organ and fecal samples were collected from 15 confiscated pangolins rescued at the Jinhua Wildlife Rescue Station in Zhejiang Province, China. Metatranscriptomic analysis combined with polymerase chain reaction (PCR) screening detected pestivirus, canine parvovirus 2 (CPV-2), human parainfluenza virus 2 (HPIV2), and *Pseudomonas aeruginosa* at high abundance in three deceased individuals, while no candidate pathogens were identified in the remaining 12 surviving animals. Two of the deceased pangolins, Pujiang-Pangolin-2 and Pujiang-Pangolin-3, were co-infected with four and two pathogens, respectively, and both exhibited more severe pathological lesions than Qingtian-Pangolin-1, in which only CPV-2 was detected. Pujiang-Pangolin-2 showed markedly elevated levels of CPV-2 and *P. aeruginosa* in the lung and spleen, accompanied by extensive tissue damage. Pujiang-Pangolin-3 had a higher abundance of pestivirus and presented with pronounced internal hemorrhage. Notably, phylogenetic analyses reveal that the pestivirus, CPV-2, and HPIV2 detected in the infected pangolins were closely related to strains previously identified in *Manis javanica*, domestic dogs from Vietnam, and humans from the Netherlands, respectively, while the *P. aeruginosa* sequences clustered with isolates obtained from human clinical samples both within China and internationally.Together with prior reports, these data suggest that trafficked pangolins are highly susceptible to diverse infections and may contribute to the transmission of zoonotic pathogens across species and geographic boundaries.

Keywords: Pangolins; Human parainfluenza virus 2; Canine parvovirus 2; Pestivirus; Co-infection

INTRODUCTION

Emerging infectious diseases caused by viruses (e.g., COVID-19, pathogenic avian influenza, and African swine fever) have had a profound impact on public health and agricultural production over the past two decades, resulting in widespread morbidity, mortality, and economic loss (Baker et al., 2022; Gaudreault et al., 2020; GBD 2021 Diseases and Injuries Collaborators, 2024). These emergent diseases are frequently initiated through cross-species transmission or “spillover” events, in which pathogens originating from wildlife successfully infect humans or domestic animal populations (Gaudreault et al., 2020; Letko et al., 2020; Wille & Holmes, 2020). Some zoonotic viruses, such as severe acute respiratory syndrome coronavirus 2 (SARS-CoV-2), have subsequently established human-to-animal and animal-to-animal transmission cycles across mammals (Oude Munnink et al., 2021). Such interspecies transmission is often facilitated by rapid viral evolution, ecological disruption, and behavioral shifts that create novel interfaces between reservoirs and susceptible hosts (Chan et al., 2013; Oude Munnink et al., 2021). In addition, large-scale movement and trafficking of wild and domestic animals accelerate the geographic dissemination of zoonotic agents and heighten the risk of pathogen emergence (Daszak et al., 2000; Lin et al., 2012).

Received: 17 September 2025; Accepted: 23 October 2025; Online: 24 October 2025

Foundation items: This study was supported by the Integovernmental International Science & Technology Innovation Cooperation (2024YFE0117100), National Natural Science Foundation of China (32130002, U22A20526, 32041004, 82341108), and Guangzhou Innovation and Entrepreneurship Team Introduction Project (2024D03J0015)

[#]Authors contributed equally to this work

*Corresponding authors, E-mail: chenyanmei@fudan.edu.cn; zhangyongzhen@fudan.edu.cn

Proactive identification and characterization of known and previously undetected zoonotic agents in wildlife reservoirs is therefore critical to mitigating future spillover risk.

Pangolins, scaly anteaters belonging to the family Manidae and order Pholidota, are native to Africa and Asia and comprise nine extant species (Gu et al., 2023; Wilson & Reeder, 2005). Habitat degradation and fragmentation have caused significant declines in pangolin populations and contraction of their historical ranges (Tee et al., 2018). Compounding this decline, pangolins are the most heavily trafficked wild mammals globally, driven by persistent demand for their meat and keratinized scales in traditional medicine markets (Gaubert et al., 2018). The detection of SARS-CoV-2-related coronaviruses in pangolin samples has intensified scrutiny of their potential role in zoonotic transmission pathways (Lam et al., 2020; Xiao et al., 2020). In the years following these initial findings, an increasing number of viral taxa have been identified in wild-caught, confiscated, and captive pangolins (Cui et al., 2023; Gao et al., 2020; Han et al., 2022; He et al., 2022; Shi et al., 2022b; Tian et al., 2022), suggesting that pangolins are natural reservoirs or hosts of multiple viruses. Several agents of clinical concern—including novel pathogens such as Dongyang pangolin virus (DYPV) and established pathogens such as canine parvovirus, respiratory syncytial virus, and rickettsial organisms—have been detected in pangolins presenting with severe illness, with some infections likely contributing to mortality (Gao et al., 2020; He et al., 2022; Li et al., 2024; Que et al., 2022; Shi et al., 2022c; Wang et al., 2020; Zhang et al., 2022). However, the origin and transmission dynamics of many of these etiological agents remain poorly understood.

In the present study, a metatranscriptomic investigation was conducted on 15 rescued pangolins, including three deceased and 12 surviving individuals, housed at the Jinhua Wildlife Rescue Station in Zhejiang Province, China. Detected pathogens associated with illness and mortality of the deceased animals were identified and molecularly characterized. In parallel, clinical observations and histopathological assessments were performed to evaluate disease manifestations and pathological changes associated with infection.

MATERIALS AND METHODS

Pangolin acquisition and sample collection

Between January and July 2019, a total of 15 trafficked pangolins were confiscated from four regions across Zhejiang Province, China—Jinhua, Lishui, Quzhou, and Wenzhou—and transported to the Jinhua Wildlife Rescue Station for medical intervention and rehabilitation (Figure 1A; Supplementary Table S1). Despite treatment, three individuals succumbed to illness, while the remaining 12 recovered and were subsequently relocated to a regional zoological facility.

To determine etiological factors associated with death, comprehensive necropsies were performed by licensed veterinarians on the deceased individuals. Tissue specimens including brain, heart, liver, lung, spleen, kidney, stomach, and intestine were aseptically harvested and stored at −80°C for downstream analysis. Fecal samples were collected from the 12 surviving pangolins and similarly preserved at −80°C. Species identification was initially based on morphological assessment by experienced field biologists and subsequently confirmed through mitochondrial cytochrome *b* (cyt *b*) gene sequencing.

All experimental procedures were reviewed and approved by the Ethics Committee of the National Institute for Communicable Disease Control and Prevention of the China Center for Disease Control and Prevention (Approval No.

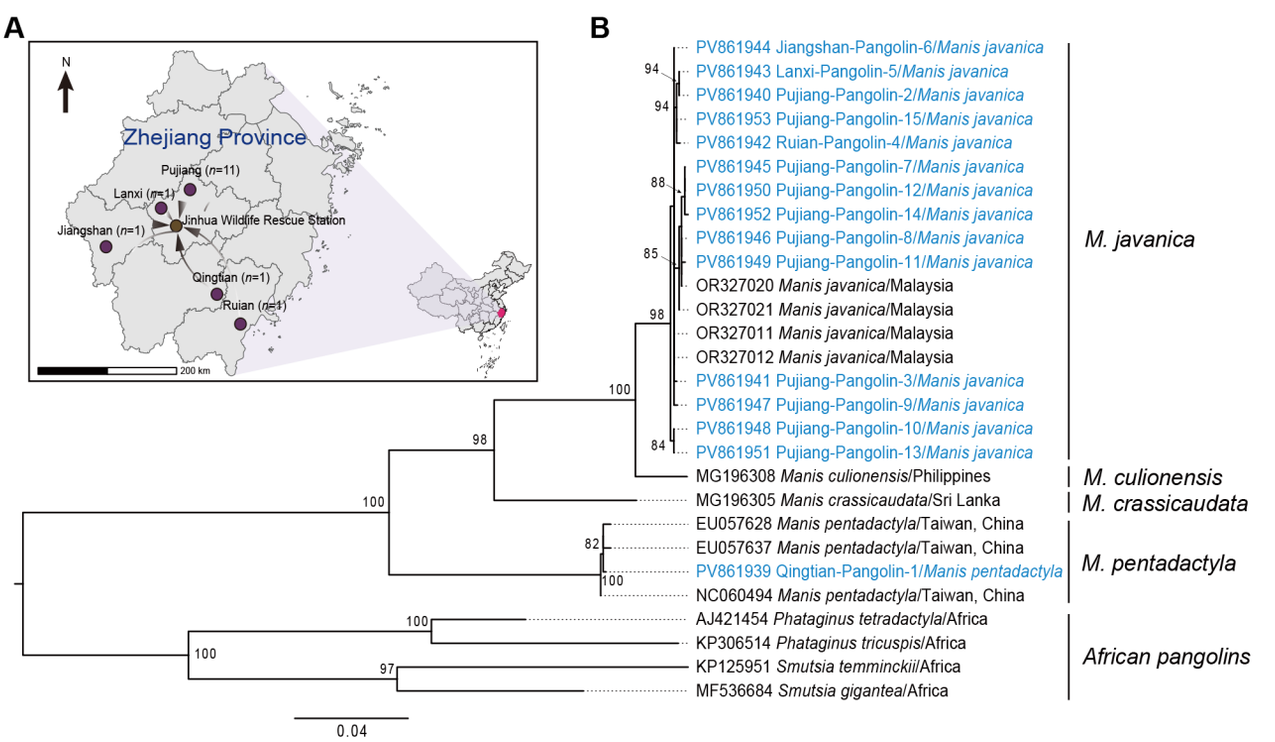

Figure 1 Genetic origin and phylogenetic relationships of rescued pangolins

A: Geographic sampling locations of rescued pangolins. B: Maximum-likelihood (ML) tree based on cyt *b* nucleotide sequences of rescued pangolins and reference pangolin taxa.

SYXK(jing)2017-0021).

Histopathological assay

Histopathological examination was performed on tissue samples (brain, heart, liver, spleen, lung, kidney, stomach, large intestine, and small intestine) collected from the three deceased pangolins. Small segments of each organ were excised using sterile surgical instruments and fixed overnight in 4% paraformaldehyde solution (Sangon Biotech, China). Fixed tissues were processed by Wuhan Servicebio Technology Co., Ltd. (China), where samples were dehydrated through a graded ethanol series, embedded in paraffin wax, and sectioned into thin slices. Sections were routinely stained with hematoxylin and eosin (H&E) and examined under a microscope for histological evaluation. Diagnostic interpretation and pathology reports were completed by a certified histopathologist.

RNA extraction, library construction, and sequencing

Total RNA was extracted from each internal organ and fecal sample using TRIzol Reagent (Invitrogen, USA) in combination with a RNeasy Plus Universal Mini Kit (Qiagen, Germany), following the manufacturers' protocols. Equal quantities of RNA from individual samples were pooled for downstream library construction (Supplementary Table S2). Libraries were generated using the TruSeq Stranded Total RNA Sample Preparation Kit (Illumina, USA), with ribosomal RNA (rRNA) removed using the Ribo-Zero^{TM} rRNA Removal Kit (Illumina, USA). Library quality was assessed on the Qsep100 system (Bioptic, China), and sequencing was performed on an Illumina NovaSeq 6000 platform (Illumina, USA) in a 150 bp paired-end manner at the Novogene Bioinformatics Institute (Novogene, China).

Screening etiological agents

Metatranscriptomic data were processed following previously described protocols (Chen et al., 2023; Shi et al., 2022a). Raw sequencing reads were quality-filtered using Trimmomatic (v.0.39) to remove adapter sequences and low-quality bases (Bolger et al., 2014). Low-complexity reads were subsequently filtered using bbduk.sh (https://sourceforge.net/projects/bbmap/), yielding high-quality clean reads. These were then aligned against the SILVA rRNA database (v.138.1) (Quast et al., 2013) and two pangolin reference genomes (GCF_030020395.1 and GCF_014570535.1) using Bowtie2 (v.2.4.5) (Langmead & Salzberg, 2012) to remove rRNA and host-derived sequences. The remaining reads were assembled *de novo* using MEGAHIT (v.1.2.9) (Li et al., 2015), followed by read mapping to the assembled contigs using Bowtie2. Read counts were quantified using SAMtools (v.1.14) (Danecek et al., 2021). Both assembled contigs and unmapped reads were searched against the NCBI non-redundant nucleotide and protein databases using BLASTn (v.2.15.0) and DIAMOND (v0.9.19.120) (Buchfink et al., 2021), with an E-value cutoff of 1×10^{-5}. Taxonomic assignments were performed using TaxonKit (v.0.15.0) (Shen & Ren, 2021) based on the top-ranked BLAST hits. Species-level abundance was calculated as reads per million (RPM) using custom R scripts.

Candidate etiological agents identified from metatranscriptomic screening were further validated using reverse transcription PCR (RT-PCR) or PCR, followed by Sanger sequencing. Viral genome reconstruction was achieved by mapping clean reads to reference genomes using Hisat2 (v.2.2.1) (Kim et al., 2019), with internal gaps filled via RT-PCR and Sanger sequencing. Terminal genomic regions were determined using rapid amplification of cDNA ends (RACE), and open reading frames (ORFs) were annotated using Geneious Prime v.2025.0.2 (https://www.geneious.com).

Quantification of etiological agent abundance in internal organs

The abundance of viral and bacterial RNA in internal tissues was quantified using TaqMan probe-based reverse transcription quantitative PCR (RT-qPCR). Specifically, target sequences from both viral and bacterial genomes were ligated into plasmid vectors to construct standard references. A 10-fold serial dilution of these plasmids, ranging from 10^3 to 10^8 copies/μL, was used to generate standard curves (Supplementary Figure S1), enabling absolute quantification of genomic targets in each tissue sample. All reactions were performed using the HiScript II One Step qRT-PCR Probe Kit (Vazyme, China) on a qTOWER3 Real-Time PCR system (Analytik Jena, Germany), with each sample analyzed in technical triplicate to ensure reproducibility.

Genetic characterization of etiological agents

Virus sequences identified in this study were aligned with representative reference genomes using the L-INS-i algorithm implemented in MAFFT (v.7.490) (Katoh & Standley, 2013). Ambiguously aligned regions were removed using TrimAl (v.1.4.rev15) (Capella-Gutiérrez et al., 2009). Maximum-likelihood (ML) phylogenetic trees were estimated based on amino acid alignments using IQ-TREE2 (v.2.2.0) (Minh et al., 2020), with 1 000 bootstrap replicates and best-fit substitution model selected by the "-m MFP" option. Branch support was considered robust at bootstrap values greater than 70%. Resulting topologies were visualized using FigTree (v.1.4.3) (http://tree.bio.ed.ac.uk/software/figtree/). Pairwise nucleotide and amino acid identities were calculated using Geneious Prime v.2025.0.2 (https://www.geneious.com).

Statistical analysis

Univariate comparisons of pathogen abundance across different tissue types within the same individual were performed using the Kruskal-Wallis *H* test, followed by Dunn's *post hoc* test. *P*-values less than 0.05 were considered statistically significant.

RESULTS

Clinical presentation and geographic origins of confiscated pangolins

Between January and July 2019, 15 trafficked pangolins were seized from five counties in Zhejiang Province, China: Lanxi (*n*=1) and Pujiang (*n*=11) in Jinhua, Qingtian (*n*=1) in Lishui, Jiangshan (*n*=1) in Quzhou, and Ruian (*n*=1) in Wenzhou. All individuals were immediately transported to the Jinhua Wildlife Rescue Station for evaluation and care (Figure 1; Supplementary Table S1). To determine species identity and infer possible geographic origins, nucleotide sequences of the cyt *b* gene were amplified from tissue or fecal samples as described previously (Gao et al., 2020). Phylogenetic analysis revealed that the individual seized in Qingtian belonged to the Chinese pangolin (*Manis pentadactyla*) and clustered most closely with sequences from Taiwan, China. The remaining 14 were identified as Malayan pangolins (*M. javanica*) and shared the highest similarity with sequences previously reported from

Malaysia (Figure 1). These findings suggest that the seized animals likely originated from Taiwan, China and Malaysia and were subsequently smuggled into mainland China.

Twelve of the pangolins appeared clinically healthy and survived rehabilitation. However, the remaining three individuals—here designated Qingtian-Pangolin-1, Pujiang-Pangolin-2, and Pujiang-Pangolin-3 based on their capture locations—developed progressive illness and ultimately died despite receiving medical treatment. Their clinical symptoms are summarized in Table 1. All three exhibited severe dermatological and gastrointestinal symptoms, including extensive skin lesions and acute diarrhea. Qingtian-Pangolin-1 showed blood blisters on the forelimbs and evidence of pharyngeal hemorrhage; Pujiang-Pangolin-2 also presented with blood blisters on both forelimbs and hindlimbs; Pujiang-Pangolin-3 exhibited hindlimb edema and hemorrhage. Blood biochemical data were only available for Pujiang-Pangolin-3, revealing thrombocytopenia, reduced concentrations of blood urea nitrogen, sodium (cNa^+), and chloride (cCl^-), alongside elevated levels of CO_2 and cholesterol.

Pathological findings in deceased pangolins

To investigate the causes of death in the three pangolins, gross anatomical examinations were conducted, and tissue specimens—including brain, heart, liver, spleen, lungs, kidneys, stomach, and both large and small intestines—were subjected to histopathological analysis. In Qingtian-Pangolin-1, the large intestine exhibited extensive mucosal epithelial loss, accompanied by mild lymphocyte infiltration in the mucosal layer (Figure 2). Intestinal glands were markedly dilated, with pronounced necrosis of glandular epithelium, which had shed into the lumen. The submucosal region showed vascular dilatation, interstitial edema, and mild lymphocyte infiltration. Similar mucosal epithelial loss and shedding were also observed in its small intestine, which displayed dilated intestinal glands and significant glandular epithelial necrosis. The spleen showed diminished white pulp and abundant hemosiderin-laden phagocytic cells. Lung sections revealed pale pink exudate occupying alveolar spaces, accompanied by occasional bronchiolar epithelial detachment and lymphocytic infiltration. Mild histological changes were observed in the liver and kidney, while no notable lesions were found in the heart, stomach, or brain (Supplementary Figure S2).

Pujiang-Pangolin-2 and Pujiang-Pangolin-3 exhibited more severe and widespread pathology than Qingtian-Pangolin-1. Both individuals presented with bilateral pulmonary atrophy, prominent lymphocytic infiltration in the submucosa of the large intestine and mucosa of the small intestine, and histological disruption in the spleen characterized by reduced lymphocytes, proliferation of trabecular structures in the red pulp, fibroblast proliferation, and scattered hemosiderin-laden macrophages (Figure 2). Furthermore, multifocal hemorrhages

Table 1 Clinical features of deceased pangolins

Pangolin	Species	Sex	Clinical features	Treatment
Qingtian-Pangolin-1	*M. pentadactyla*	Male	Skin lesions, bleeding, blood blisters, acute diarrhea	Antibiotics
Pujiang-Pangolin-2	*M. javanica*	Female	Skin lesions, blood blisters, acute diarrhea	Montmorillonite, antibiotics
Pujiang-Pangolin-3	*M. javanica*	Male	Skin lesions, edema, bleeding, acute diarrhea	Montmorillonite, antibiotics

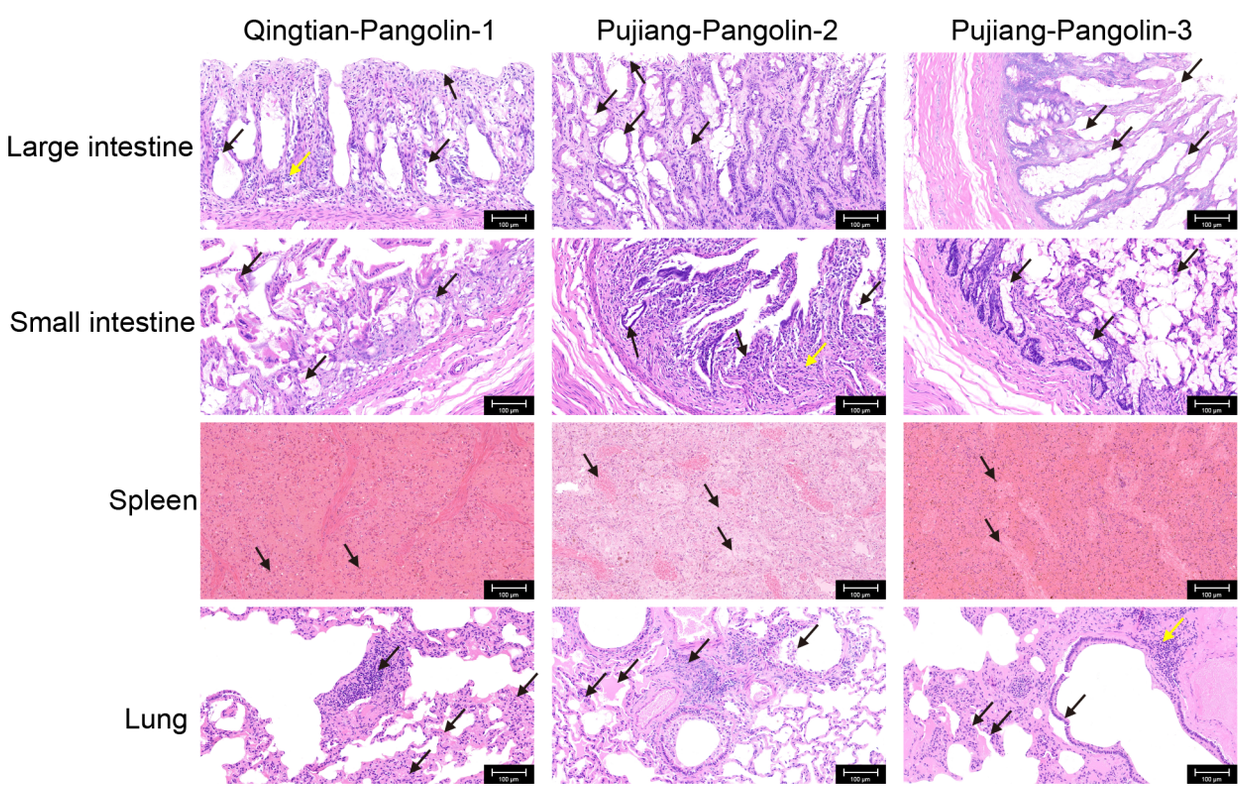

Figure 2 Pathological lesions in deceased pangolins

Histopathological changes in lung, spleen, and large and small intestines of Qingtian-Pangolin-1, Pujiang-Pangolin-2, and Pujiang-Pangolin-3, showing lymphocytic infiltration (yellow arrows) and other lesions (black arrows).

were evident in the liver, spleen, lung, and kidney of Pujiang-Pangolin-3, and eosinophilic exudate was present in the lumen of the small intestine (Figure 2; Supplementary Figure S2). Mild histopathological changes were also observed in the heart and liver of Pujiang-Pangolin-2, and in the liver and kidney of Pujiang-Pangolin-3 (Supplementary Figure S2).

Identification and distribution of etiological agents in deceased pangolins

To identify potential etiological agents responsible for the observed disease and mortality, RNA was extracted from the lung, liver, kidney, spleen, brain, and heart tissues, as well as from intestinal feces, of each deceased pangolin. Based on previously established protocols (Chen et al., 2023; Gao et al., 2020; Shi et al., 2022a), RNA from internal organs of the same individual was pooled to generate three organ-derived sequencing libraries, while fecal RNA was used to generate three separate fecal libraries. Consequently, a total of 993 699 182 sequence reads were obtained, among which 26 839 034 clean reads were retained for downstream *de novo* assembly. Assembly results revealed the presence of canine parvovirus 2 (CPV-2) in Qingtian-Pangolin-1, with abundances of 2 855.25 RPM in the fecal library and 1 781.43 RPM in the internal organ library (Supplementary Table S2). In Pujiang-Pangolin-2, co-infection with CPV-2, pestivirus, and human parainfluenza virus 2 (HPIV2) was detected, with RPM values of 5 298.52 and 12.92 for CPV-2, 2 709.38 and 169.22 for pestivirus, and 80.91 and 649.76 for HPIV2 in fecal and organ libraries, respectively. Pujiang-Pangolin-3 harbored both HPIV2 and pestivirus, with RPM values of 31.93 and 69.17 for HPIV2 and 1 425.51 and 2 760.77 for pestivirus in fecal and organ libraries, respectively. No known animal or human pathogens were detected in fecal samples from the 12 surviving pangolins.

Given the presence of multi-organ damage in deceased pangolins, further evaluation of pathogen tissue distribution was performed by RT-qPCR (Supplementary Table S3) (Chen et al., 2016; Deng et al., 2018; Jolley et al., 2018; Niikura et al., 2021; Rodríguez-Díaz et al., 2009; Tong et al., 2008; Wang et al., 2015). Notably, significant variation in viral loads across different tissues was observed for all four pathogens (Kruskal-Wallis *H* test, all $P<0.01$; Figure 3; Supplementary Table S4). CPV-2 was most abundant in the intestine and spleen of both Qingtian-Pangolin-1 and Pujiang-Pangolin-2, although viral RNA was also detected in other organs (Figure 3A; Supplementary Tables S4, S5). Pestivirus was distributed broadly in Pujiang-Pangolin-2 and Pujiang-Pangolin-3, with high loads in the intestine, kidney, spleen, and lung, and a peak concentration of 5.08×10^8 copies/μL in the spleen of Pujiang-Pangolin-3 (Figure 3B; Supplementary Tables S4, S5). The spatial distribution of CPV-2 and pestivirus was consistent with clinical symptoms (e.g., diarrhea) and the histopathological findings. HPIV2 was detected at higher abundance in the brain (9.00×10^6 copies/μL) of Pujiang-Pangolin-2 and in the lung (3.06×10^8 copies/μL) of Pujiang-Pangolin-3, with lower levels in the intestine, heart, stomach, and spleen, and undetectable levels in the liver and kidney (Figure 3C; Supplementary Tables S4, S5).

Beyond viral pathogens, additional screening by RT-qPCR targeted non-viral agents with high metatranscriptomic abundance. *Pseudomonas aeruginosa* was predominantly detected in the lung, heart, spleen, and brain of Pujiang-Pangolin-2, with lower concentrations in other organs (Figure 3D; Supplementary Tables S4, S5), consistent with its elevated abundance (237 401.68 RPM) in the corresponding organ-derived library (Supplementary Table S2). These findings implicate *P. aeruginosa* as a likely contributor to systemic infection in this individual. Other bacterial species were also present in the internal organ libraries but were excluded from further analysis due to low abundance, absence in RT-qPCR assays, or classification as likely commensals.

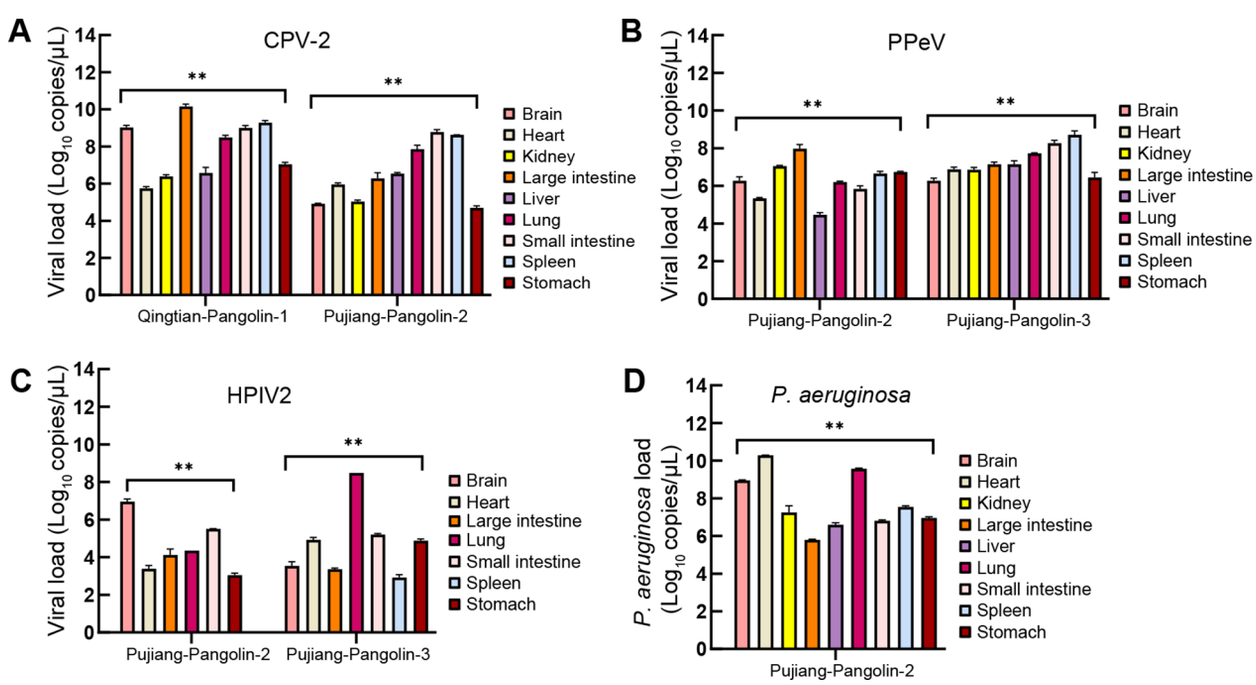

Figure 3 Tissue distribution of pathogen abundance in three deceased pangolins, as determined by qRT-PCR

Abundances of CPV-2 VP2 gene, PPeV NS3 gene, HPIV2 HN gene, and *P. aeruginosa* 23S rRNA gene were measured. Samples with undetectable fluorescence signals are not shown. **: $P<0.01$.

Genetic characterization of viral and bacterial pathogens identified in pangolins

Two near-complete pestivirus genomes, designated PPeV PJP2 and PPeV PJP3, were recovered from Pujiang-Pangolin-2 and Pujiang-Pangolin-3, respectively. These genomes shared 99.96% nucleotide identity (Supplementary Table S6) and exhibited closest homology to Pangolin pestivirus BIME6 (URZ29368.1), previously identified in deceased *M. javanica* from Guangxi Province, China (Shi et al., 2022b), with 93.53% nucleotide and 95.45% amino acid similarity. In contrast, they were more distantly related to DYPV, recovered from a deceased *M. javanica* rescued at the same station in 2018 (Gao et al., 2020), sharing only 74.85% nucleotide and 81.47% amino acid identity. Phylogenetic analysis based on polyprotein and NS3 amino acid sequences (Figure 4) grouped all pangolin-derived pestiviruses into two distinct clades, corresponding to DYPV and an undefined lineage. These clades appear host-specific, associated with *M. javanica* and *M. pentadactyla*, respectively. Within clade I, pangolin-associated pestiviruses displayed substantial genetic diversity. The viruses identified in this study clustered within a single lineage together with BIME6, followed by Pangolin pestivirus 2, Pangolin pestivirus 3, and BIME7, indicating a closely related evolutionary group within this clade (He et al., 2022; Shi et al., 2022b).

Two near-complete genomes of CPV-2, termed CPV QTP1 and CPV PJP2, were recovered from Qingtian-Pangolin-1 and Pujiang-Pangolin-2, respectively. These genomes were identical at the nucleotide level (100% similarity) (Supplementary Table S7) and exhibited closest phylogenetic relatedness to parvoviruses isolated from domestic dogs in Vietnam (OK094438 and LC214969), pangolins in Taiwan, China (MN832850) (Wang et al., 2020), and unassigned host samples from Heilongjiang Province, China (PP035131 and PP035148). Phylogenetic trees constructed from full-genome and VP2 gene sequences (Figure 5A) placed all these viruses within the Asian CPV-2c lineage. Comparative genomic analysis revealed only a limited number of nucleotide substitutions between pangolin-derived CPV-2 and those from dogs and pangolins in nearby regions, none of which were nonsynonymous (Figure 5B).

Two near-complete genomes of HPIV2, named HPIV2 PJP2 and HPIV2 PJP3, were recovered from Pujiang-Pangolin-2 and Pujiang-Pangolin-3, respectively. These sequences were identical at the nucleotide level (100% similarity) (Supplementary Table S8) and shared 99.8% similarity with HPIV2 previously detected in deceased trafficked pangolins (He et al., 2022). Furthermore, the sequences showed ≥ 99.57% nucleotide identity with strains circulating in human populations both within China and internationally (Kennedy et al., 2017; Mansour et al., 2024; Phan et al., 2019; Zhu et al., 2024). In the phylogenetic trees based on whole-genome and RdRp gene sequences (Figure 6A), all pangolin-associated HPIV2 clustered within a distinct lineage of the G1a genotype and shared a close evolutionary relationship with human HPIV2 strains sampled from the Netherlands, Russia, USA, and China. Comparative sequence analysis revealed 13 consistent nucleotide differences relative to closely related human HPIV2, including two nonsynonymous mutations: T138A in the N-terminal domain of the V protein and R542Q in the RdRp domain of the L protein (Figure 6B, C; Supplementary Figure S3). These substitutions may reflect adaptive changes enabling cross-species transmission into pangolins, analogous to host-switching mutations described in SARS-CoV-2 (Lv et al., 2024).

To characterize the genetic identity of *P. aeruginosa* detected in Pujiang-Pangolin-2, seven housekeeping genes (*acsA*, *aroE*, *guaA*, *mutL*, *nuoD*, *ppsA*, and *trpE*) were amplified from lung tissue and subjected to multilocus sequence typing. Phylogenetic analysis of concatenated sequences confirmed the strain belonged to the ST357 genotype and showed high similarity to *P. aeruginosa* isolates derived from human infections worldwide (Supplementary Figure S4).

DISCUSSION

Over the past six years, frequent reports have documented the deaths of trafficked pangolins housed in wildlife rescue stations (Gao et al., 2020; Li et al., 2024; Que et al., 2022; Shi et al., 2022c; Wang et al., 2020; Zhang et al., 2022). A variety of microbial agents, including bacteria, parasites, and viruses, have been identified in affected individuals and are considered likely contributors to clinical deterioration and mortality. In most previously reported cases, only a single pathogen was detected per individual (Gao et al., 2020; He et al., 2022). In contrast, the present study identified four distinct

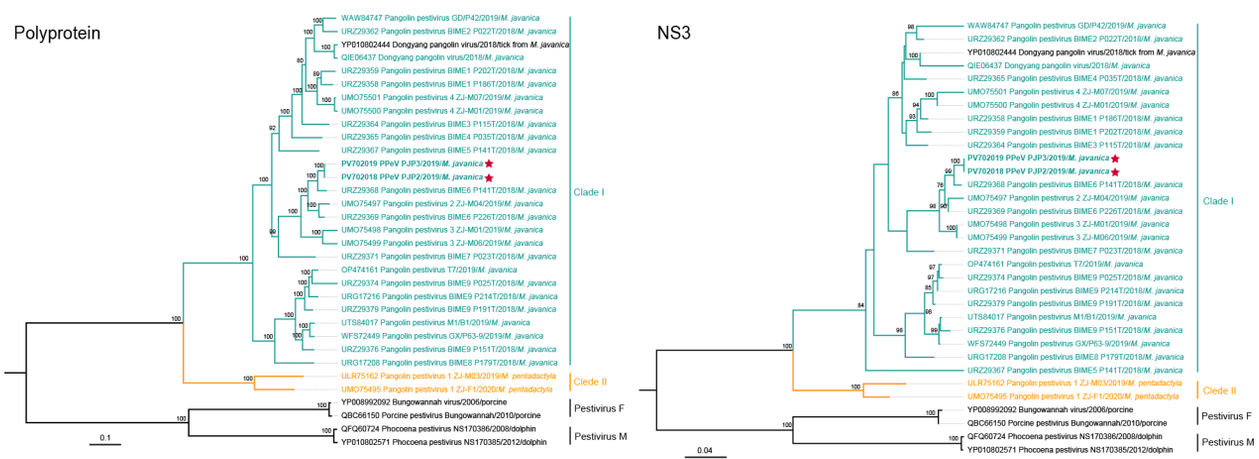

Figure 4 Phylogenetic relationships of PPeV detected in pangolins

Maximum-likelihood (ML) trees were constructed using amino acid sequences of the complete coding region (polyprotein) and the NS3 gene, and midpoint-rooted for visualization. Viruses identified in this study are noted with a red star.

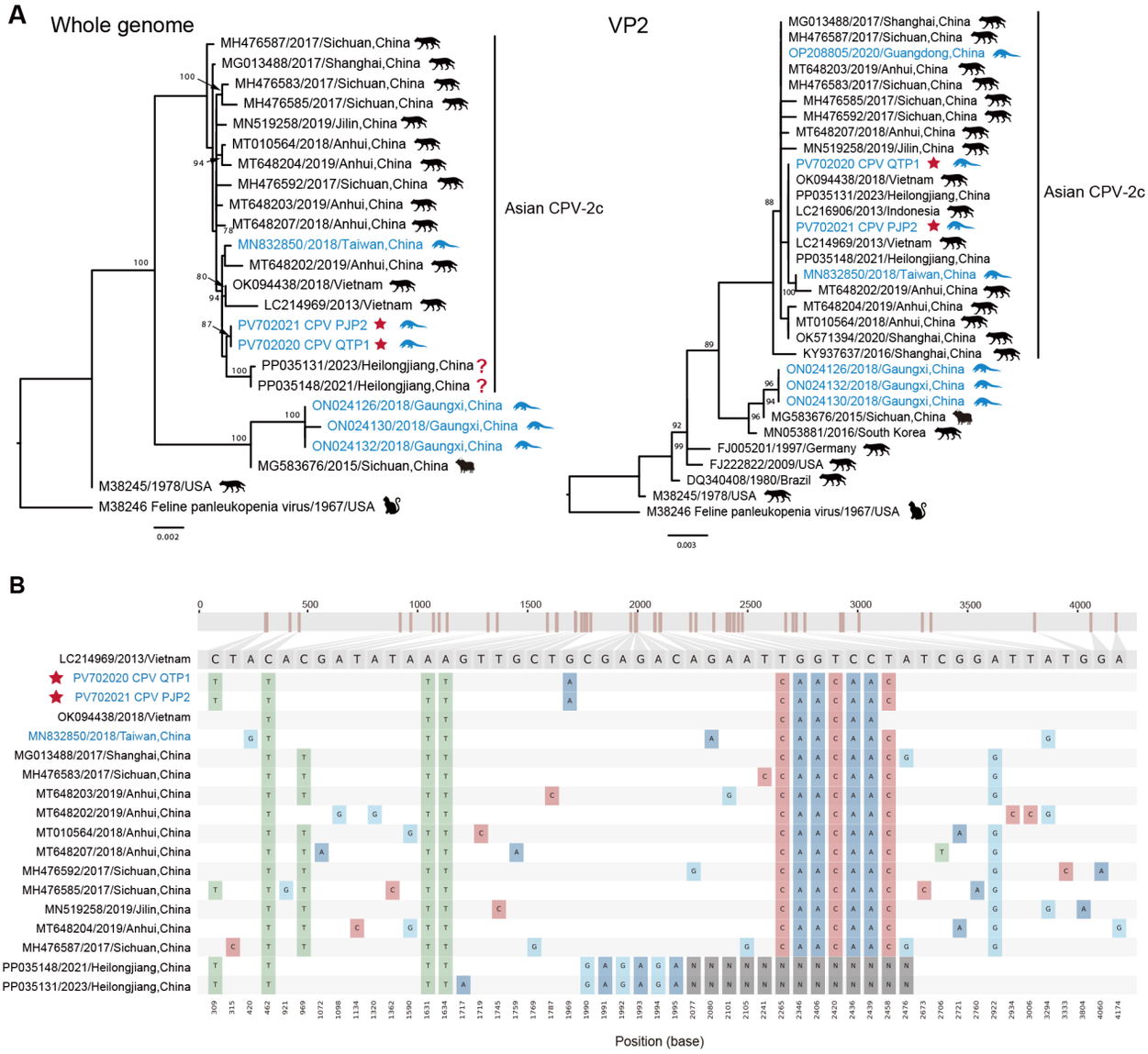

Figure 5 Phylogenetic relationships and genomic features of CPV-2 detected in pangolins

A: Maximum-likelihood (ML) trees based on whole-genome and VP2 gene nucleotide sequences of two pangolin CPV-2 isolates and reference strains, rooted with Feline panleukopenia virus. B: Nucleotide differences between two pangolin CPV-2 isolates and their 16 closest canine strains, using the closest relative as reference. Pangolin-derived viruses are shown in blue; newly identified viruses are noted with a red star.

pathogens—CPV-2, pestivirus, HPIV2, and *P. aeruginosa*—in three deceased trafficked pangolins, all at high abundance. Given their close genetic similarity to established mammalian pathogens, these agents likely played a causative role in disease development and death. Notably, CPV-2, HPIV2, pestivirus, and *P. aeruginosa* co-occurred in Pujiang-Pangolin-2, while HPIV2 and pestivirus were simultaneously present in Pujiang-Pangolin-3, indicating multi-pathogen co-infection. Although only CPV-2 was detected in Qingtian-Pangolin-1, these findings collectively suggest that trafficked pangolins are highly susceptible to diverse infections, potentially due to stress-induced immunosuppression and abrupt environmental changes during trafficking. In addition, while SARS-CoV-2-related coronaviruses have previously been identified in pangolins trafficked from Southeast Asia (Lam et al., 2020; Nga et al., 2022; Peng et al., 2021; Xiao et al., 2020), no such viruses were detected in the present cohort, implying that these animals likely originated from different geographic regions.

Pestiviruses are recognized as major pathogens in domestic animals and have recently been detected in a broad range of wildlife hosts, including bats and rodents (Postel et al., 2021). Since the first identification of DYPV in a deceased *M. javanica* individual (Gao et al., 2020), increasing pestivirus diversity has been described in both diseased and apparently healthy pangolins (Cui et al., 2023; He et al., 2022; Shi et al., 2022b, 2022c; Tian et al., 2022). Notably, phylogenetic analyses demonstrated that all pangolin-derived pestiviruses formed a monophyletic group with high internal diversity (Figure 4). All clade I pestiviruses have been exclusively associated with *M. javanica*, except for one virus detected in a tick collected from a deceased *M. javanica* (Gao et al., 2020), while clade II viruses have thus far been confined to *M. pentadactyla*. These patterns suggest a long-standing co-evolutionary relationship between pestiviruses and their pangolin hosts, with the lineages identified here likely originating from Malaysia. In our previous study, DYPV was associated with hemorrhagic lesions in *M. javanica* (Gao et al.,

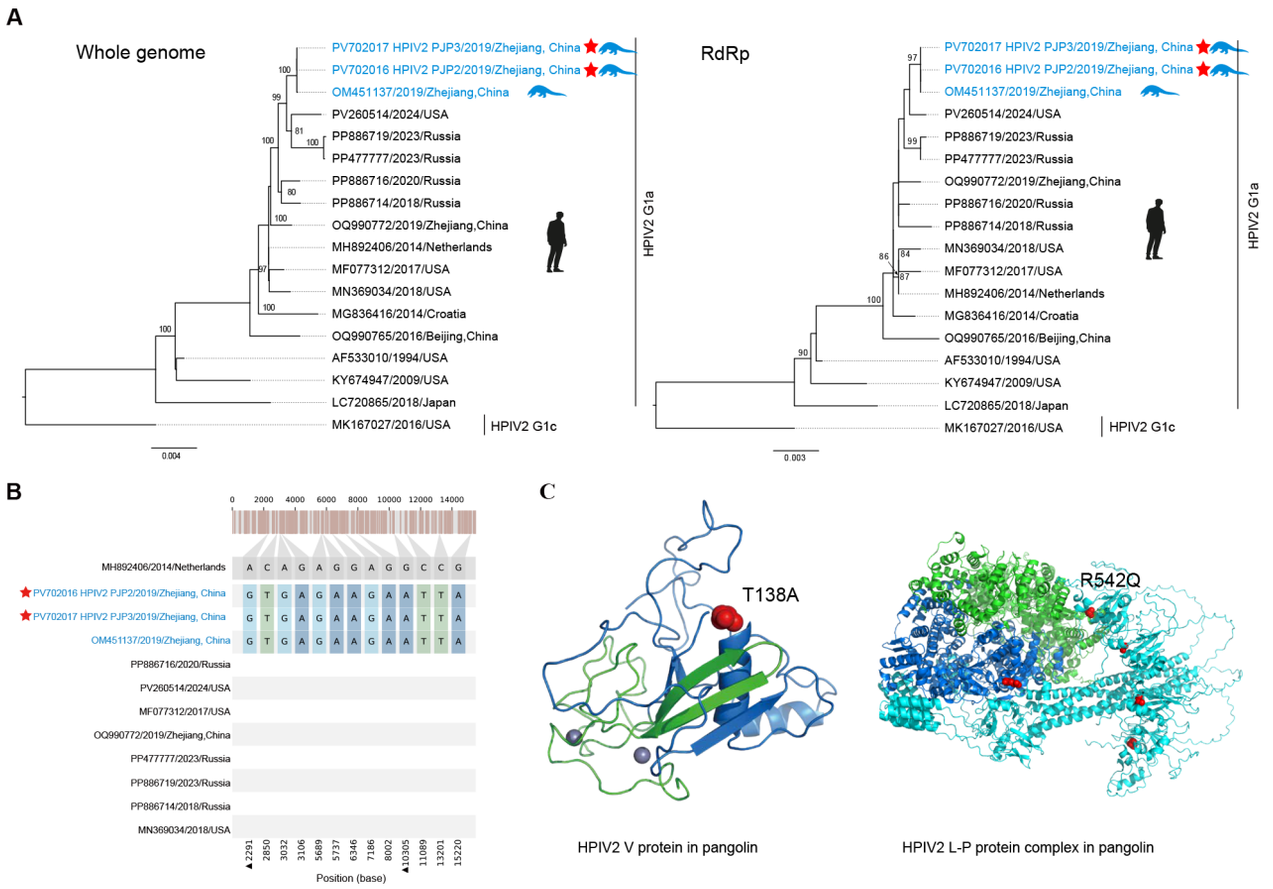

Figure 6 Phylogenetic relationships and genomic features of HPIV2 detected in pangolins

A: Maximum-likelihood (ML) trees were constructed based on whole-genome sequences and the RdRp domain within the L gene of HPIV2 PJP and other known HPIV2 strains, rooted with HPIV2 G1c. Pangolin-derived viruses are shown in blue; newly identified strains are noted with a red star. B: Genomic nucleotide divergence between two pangolin-derived HPIV2 strains and their 10 closest human-derived strains, using the closest human sequence as reference. Only nucleotide sites conserved among all pangolin sequences but absent in all human sequences were shown here. Nonsynonymous mutations are marked with triangles. Full mutation spectrum is provided in Supplementary Figure S3. C: Predicted structural models of the V protein and L-P protein complex from the pangolin HPIV2 genome. Mutations are indicated as red spheres. The V protein structure was predicted using SWISS-MODEL (https://swissmodel.expasy.org/) with PDB entry 2hye.1.B as the primary template. The L-P protein complex structure was predicted *de novo* using AlphaFold (https://alphafoldserver.com/).

2020). In the present study, similar hemorrhagic pathology was observed in Pujiang-Pangolin-2 and Pujiang-Pangolin-3, further implicating pangolin-associated pestiviruses in hemorrhagic disease. Notably, pestivirus abundance was higher in both intestinal and systemic tissues of Pujiang-Pangolin-3 compared to Pujiang-Pangolin-2 (Figure 3; Supplementary Table S2), which may account for the more severe hemorrhagic presentation observed in the former.

CPV-2 and its antigenic variants are globally prevalent among domestic and wild carnivores and are recognized for causing enteric and systemic infections with high morbidity and mortality (Miranda & Thompson, 2016). Recent studies have reported CPV-2 infection in deceased pangolins, often accompanied by severe gastrointestinal manifestations (Chang et al., 2021; Wang et al., 2020; Zhang et al., 2022). Similar to CPV-2-infected canids, pangolins infected with CPV-2 exhibited acute diarrhea and marked intestinal pathology. In this study, CPV-2 sequences recovered from pangolin tissues clustered within the 2c lineage and showed high genetic similarity to viral strains circulating in local dog populations (Figure 5), suggesting cross-species transmission from sympatric canids. Qingtian-Pangolin-1, in particular, showed extensive mucosal damage and epithelial necrosis in both the small and large intestines. Additional findings included splenic white pulp depletion with hemosiderin-laden phagocytes and alveolar spaces filled with pale pink exudate in the lungs (Figure 2). These lesions were consistent with systemic viral dissemination, further supported by high CPV-2 abundance across multiple organs (Figure 3A), indicating widespread multisystemic infection.

HPIV2, classified within the genus *Orthorubulavirus* of the subfamily *Rubulavirinae*, is an established respiratory pathogen in humans and is associated with severe respiratory tract illness in both pediatric and adult populations (Farahmand et al., 2021). The recent recovery and identification of HPIV2 in pangolins (He et al., 2022) raises concerns about human-to-wildlife transmission. In this study, HPIV2 was detected at high abundance in the brain of Pujiang-Pangolin-2 and in the lung of Pujiang-Pangolin-3, with comparatively lower abundance in other organs (Figure 3C). Notably, genomic analysis showed that these viruses were highly similar (≥99.57% nucleotide identity) to strains previously detected in pangolins (He et al., 2022) and to those circulating in human populations worldwide (Kennedy et al., 2017; Mansour et al., 2024; Phan et al., 2019; Zhu et al., 2024). These findings indicate that HPIV2 is capable of

infecting pangolins under natural conditions, most likely via spillover from infected humans. The detection of high viral loads in extra-respiratory tissues further supports the potential for systemic infection in this nonhuman host (Farahmand et al., 2021).

In addition to viral agents, *P. aeruginosa* was also detected at high abundance in the lungs and heart of Pujiang-Pangolin-2. Co-infection involving CPV-2, pestivirus, HPIV2, and *P. aeruginosa* in Pujiang-Pangolin-2, and concurrent infection with pestivirus and HPIV2 in Pujiang-Pangolin-3, likely contributed to the more extensive histopathological damage observed in these two individuals relative to Qingtian-Pangolin-1.

Although these data strongly implicate multiple pathogens in the observed disease phenotypes, the limited sample size and lack of internal organ sequencing data from healthy pangolins constrain definitive conclusions. Further investigations are necessary to establish the pathogenic potential of these agents in pangolins, and to assess the susceptibility of trafficked pangolins to zoonotic infection and their role in pathogen spillover dynamics.

DATA AVAILABILITY

The cyt *b* sequences of the rescued pangolins and the newly identified viral sequences were deposited in GenBank (accession numbers PV861939-PV861953 and PV702016-PV702021, respectively). The RNA-seq reads were deposited in the Science Data Bank (Data DOI: https://doi.org/10.57760/sciencedb.j00139.00289), Genome Sequence Archive (accession number PRJCA040769), and NCBI Sequence Read Archive (BioProjectID PRJNA1268693).

SUPPLEMENTAL DATA

Supplementary data to this article can be found online.

COMPETING INTERESTS

The authors declare that they have no competing interests.

AUTHORS' CONTRIBUTION

Y.Z.Z. conceived, designed, and led the study. X.D.L. and H.F.M. performed sample collection. S.W.Q., J.X.L., M.Q.L., Y.Y.P., X.L., and X.Q.L. performed the experiments. S.W.Q. and Y.M.C. analyzed the data. X.D.L., S.W.Q., J.X.L., Y.M.C., and Y.Z.Z. drafted the manuscript. Y.M.C. and Y.Z.Z. revised the manuscript and validated the data. All authors read and approved the final version of the manuscript.

REFERENCES

Baker RE, Mahmud AS, Miller IF, et al. 2022. Infectious disease in an era of global change. *Nature Reviews Microbiology*, **20**(4): 193–205.

Bolger AM, Lohse M, Usadel B. 2014. Trimmomatic: a flexible trimmer for Illumina sequence data. *Bioinformatics*, **30**(15): 2114–2120.

Buchfink B, Reuter K, Drost HG. 2021. Sensitive protein alignments at tree-of-life scale using DIAMOND. *Nature Methods*, **18**(4): 366–368.

Capella-Gutiérrez S, Silla-Martínez JM, Gabaldón T. 2009. trimAl: a tool for automated alignment trimming in large-scale phylogenetic analyses. *Bioinformatics*, **25**(15): 1972–1973.

Chan JFW, To KKW, Tse H, et al. 2013. Interspecies transmission and emergence of novel viruses: lessons from bats and birds. *Trends in Microbiology*, **21**(10): 544–555.

Chang YC, Lin ZY, Lin YX, et al. 2021. Canine parvovirus infections in Taiwanese pangolins (*Manis pentadactyla pentadactyla*). *Veterinary Pathology*, **58**(4): 743–750.

Chen LJ, Lin XD, Guo WP, et al. 2016. Diversity and evolution of avian influenza viruses in live poultry markets, free-range poultry and wild wetland birds in China. *Journal of General Virology*, **97**(4): 844–854.

Chen YM, Hu SJ, Lin XD, et al. 2023. Host traits shape virome composition and virus transmission in wild small mammals. *Cell*, **186**(21): 4662–4675. e12.

Cui XY, Fan KW, Liang XH, et al. 2023. Virus diversity, wildlife-domestic animal circulation and potential zoonotic viruses of small mammals, pangolins and zoo animals. *Nature Communications*, **14**(1): 2488.

Danecek P, Bonfield JK, Liddle J, et al. 2021. Twelve years of SAMtools and BCFtools. *GigaScience*, **10**(2): giab008.

Daszak P, Cunningham AA, Hyatt AD. 2000. Emerging infectious diseases of wildlife--threats to biodiversity and human health. *Science*, **287**(5452): 443–449.

Deng XY, Zhang JL, Su JZ, et al. 2018. A multiplex PCR method for the simultaneous detection of three viruses associated with canine viral enteric infections. *Archives of Virology*, **163**(8): 2133–2138.

Farahmand M, Shatizadeh Malekshahi S, Jabbari MR, et al. 2021. The landscape of extrapulmonary manifestations of human parainfluenza viruses: a systematic narrative review. *Microbiology and Immunology*, **65**(1): 1–9.

Gao WH, Lin XD, Chen YM, et al. 2020. Newly identified viral genomes in pangolins with fatal disease. *Virus Evolution*, **6**(1): veaa020.

Gaubert P, Antunes A, Meng H, et al. 2018. The complete phylogeny of pangolins: scaling up resources for the molecular tracing of the most trafficked mammals on Earth. *Journal of Heredity*, **109**(4): 347–359.

Gaudreault NN, Madden DW, Wilson WC, et al. 2020. African swine fever virus: an emerging DNA arbovirus. *Frontiers in Veterinary Science*, **7**: 215.

GBD 2021 Diseases and Injuries Collaborators. 2024. Global incidence, prevalence, years lived with disability (YLDs), disability-adjusted life-years (DALYs), and healthy life expectancy (HALE) for 371 diseases and injuries in 204 countries and territories and 811 subnational locations, 1990–2021: a systematic analysis for the Global Burden of Disease Study 2021. *The Lancet*, **403**(10440): 2133–2161.

Gu TT, Wu H, Yang F, et al. 2023. Genomic analysis reveals a cryptic pangolin species. *Proceedings of the National Academy of Sciences of the United States of America*, **120**(40): e2304096120.

Han ZZ, Xiao JB, Song Y, et al. 2022. Highly diverse ribonucleic acid viruses in the viromes of eukaryotic host species in Yunnan province, China. *Frontiers in Microbiology*, **13**: 1019444.

He WT, Hou X, Zhao J, et al. 2022. Virome characterization of game animals in China reveals a spectrum of emerging pathogens. *Cell*, **185**(7): 1117–1129. e8.

Jolley KA, Bray JE, Maiden MCJ. 2018. Open-access bacterial population genomics: BIGSdb software, the PubMLST. org website and their applications. *Wellcome Open Research*, **3**: 124.

Katoh K, Standley DM. 2013. MAFFT multiple sequence alignment software version 7: improvements in performance and usability. *Molecular Biology and Evolution*, **30**(4): 772–780.

Kennedy JL, Kincaid JC, Schwalm KC, et al. 2017. Genome sequences of three novel isolates of human parainfluenza virus 2 associated with acute respiratory infection. *Genome Announcements*, **5**(33): e00784–17.

Kim D, Paggi JM, Park C, et al. 2019. Graph-based genome alignment and genotyping with HISAT2 and HISAT-genotype. *Nature Biotechnology*, **37**(8): 907–915.

Lam TTY, Jia N, Zhang YW, et al. 2020. Identifying SARS-CoV-2-related coronaviruses in Malayan pangolins. *Nature*, **583**(7815): 282–285.

Langmead B, Salzberg SL. 2012. Fast gapped-read alignment with Bowtie 2. *Nature Methods*, **9**(4): 357–359.

Letko M, Seifert SN, Olival KJ, et al. 2020. Bat-borne virus diversity, spillover and emergence. *Nature Reviews Microbiology*, **18**(8): 461–471.

Li B, Zhai JQ, Wu YJ, et al. 2024. Molecular identification of tick-borne *Rickettsia, Anaplasma, Ehrlichia, Babesia*, and *Colpodella* in confiscated

Malayan pangolins. *PLoS Neglected Tropical Diseases*, **18**(11): e0012667.
Li DH, Liu CM, Luo RB, et al. 2015. MEGAHIT: an ultra-fast single-node solution for large and complex metagenomics assembly via succinct *de Bruijn* graph. *Bioinformatics*, **31**(10): 1674–1676.
Lin XD, Guo WP, Wang W, et al. 2012. Migration of Norway rats resulted in the worldwide distribution of Seoul hantavirus today. *Journal of Virology*, **86**(2): 972–981.
Lv JX, Liu X, Pei YY, et al. 2024. Evolutionary trajectory of diverse SARS-CoV-2 variants at the beginning of COVID-19 outbreak. *Virus Evolution*, **10**(1): veae020.
Mansour O, Fadeev AV, Perederiy AA, et al. 2024. Development of primer panels for amplicon sequencing of human parainfluenza viruses type 1 and 2. *International Journal of Molecular Sciences*, **25**(23): 13119.
Minh BQ, Schmidt HA, Chernomor O, et al. 2020. IQ-TREE 2: new models and efficient methods for phylogenetic inference in the genomic era. *Molecular Biology and Evolution*, **37**(5): 1530–1534.
Miranda C, Thompson G. 2016. Canine parvovirus: the worldwide occurrence of antigenic variants. *Journal of General Virology*, **97**(9): 2043–2057.
Nga NTT, Latinne A, Thuy HB, et al. 2022. Evidence of SARS-CoV-2 related coronaviruses circulating in Sunda pangolins (*Manis javanica*) confiscated from the illegal wildlife trade in Viet Nam. *Frontiers in Public Health*, **10**: 826116.
Niikura M, Atobe S, Takahashi A, et al. 2021. Development of a rapid and sensitive analytical system for *Pseudomonas aeruginosa* based on reverse transcription quantitative PCR targeting of rRNA molecules. *Emerging Microbes & Infections*, **10**(1): 677–686.
Oude Munnink BB, Sikkema RS, Nieuwenhuijse DF, et al. 2021. Transmission of SARS-CoV-2 on mink farms between humans and mink and back to humans. *Science*, **371**(6525): 172–177.
Peng MS, Li JB, Cai ZF, et al. 2021. The high diversity of SARS-CoV-2-related coronaviruses in pangolins alerts potential ecological risks. *Zoological Research*, **42**(6): 834–844.
Phan MVT, Arron G, Geurtsvankessel CH, et al. 2019. Complete genome characterization of eight human parainfluenza viruses from the Netherlands. *Microbiology Resource Announcements*, **8**(15): e00125–19.
Postel A, Smith DB, Becher P. 2021. Proposed update to the taxonomy of pestiviruses: eight additional species within the genus *Pestivirus*, family *Flaviviridae*. *Viruses*, **13**(8): 1542.
Quast C, Pruesse E, Yilmaz P, et al. 2013. The SILVA ribosomal RNA gene database project: improved data processing and web-based tools. *Nucleic Acids Research*, **41**(D1): D590–D596.
Que TC, Li J, He YG, et al. 2022. Human parainfluenza 3 and respiratory syncytial viruses detected in pangolins. *Emerging Microbes & Infections*, **11**(1): 1657–1663.
Rodríguez-Díaz J, Querales L, Caraballo L, et al. 2009. Detection and characterization of waterborne gastroenteritis viruses in urban sewage and sewage-polluted river waters in Caracas, Venezuela. *Applied and Environmental Microbiology*, **75**(2): 387–394.
Shen W, Ren H. 2021. TaxonKit: a practical and efficient NCBI taxonomy toolkit. *Journal of Genetics and Genomics*, **48**(9): 844–850.
Shi M, Zhao S, Yu B, et al. 2022a. Total infectome characterization of respiratory infections in pre-COVID-19 Wuhan, China. *PLoS Pathogens*, **18**(2): e1010259.
Shi WQ, Shi M, Que TC, et al. 2022b. Trafficked Malayan pangolins contain viral pathogens of humans. *Nature Microbiology*, **7**(8): 1259–1269.
Shi YN, Li LM, Zhou JB, et al. 2022c. Detection of a novel *Pestivirus* strain in Java ticks (*Amblyomma javanense*) and the hosts Malayan pangolin (*Manis javanica*) and Chinese pangolin (*Manis pentadactyla*). *Frontiers in Microbiology*, **13**: 988730.
Tee SL, Samantha LD, Kamarudin N, et al. 2018. Urban forest fragmentation impoverishes native mammalian biodiversity in the tropics. *Ecology and Evolution*, **8**(24): 12506–12521.
Tian FJ, Li J, Liu WL, et al. 2022. Virome in healthy pangolins reveals compatibility with multiple potentially zoonotic viruses. *Zoological Research*, **43**(6): 977–988.
Tong SX, Chern SWW, Li Y, et al. 2008. Sensitive and broadly reactive reverse transcription-PCR assays to detect novel paramyxoviruses. *Journal of Clinical Microbiology*, **46**(8): 2652–2658.
Wang SL, Tu YC, Lee MS, et al. 2020. Fatal canine parvovirus-2 (CPV-2) infection in a rescued free-ranging Taiwanese pangolin (*Manis pentadactyla pentadactyla*). *Transboundary and Emerging Diseases*, **67**(3): 1074–1081.
Wang W, Lin XD, Guo WP, et al. 2015. Discovery, diversity and evolution of novel coronaviruses sampled from rodents in China. *Virology*, **474**: 19–27.
Wille M, Holmes EC. 2020. Wild birds as reservoirs for diverse and abundant gamma- and deltacoronaviruses. *FEMS Microbiology Reviews*, **44**(5): 631–644.
Wilson DE, Reeder DM. 2005. Mammal Species of the World: A Taxonomic and Geographic Reference. 3rd ed. Baltimore: Johns Hopkins University Press.
Xiao KP, Zhai JQ, Feng YY, et al. 2020. Isolation of SARS-CoV-2-related coronavirus from Malayan pangolins. *Nature*, **583**(7815): 286–289.
Zhang LN, Wang K, An FY, et al. 2022. Fatal canine parvovirus type 2a and 2c infections in wild Chinese pangolins (*Manis pentadactyla*) in southern China. *Transboundary and Emerging Diseases*, **69**(6): 4002–4008.
Zhu Y, Sun Y, Li CC, et al. 2024. Genetic characteristics of human parainfluenza viruses 1–4 associated with acute lower respiratory tract infection in Chinese children, during 2015–2021. *Microbiology Spectrum*, **12**(10): e03432–23.